Viscoelastic solutions for conical indentation

Matthieu Vandamme, Franz-Josef Ulm *

Massachusetts Institute of Technology, CEE 1-263, 77 Massachusetts Avenue, Cambridge, MA 02139, United States

Abstract

The aim of indentation analysis is to link indentation data, typically an indentation force vs. indentation depth curve, *P–h*, to meaningful mechanical properties of the indented material. While well established for time independent behavior, the presence of a time dependent behavior can strongly affect both the loading and the unloading responses. The paper presents a framework of viscoelastic indentation analysis based on the method of functional equations, developed by Lee and Radok [1960, The contact problem for viscoelastic bodies, J. Appl. Mech. 27, 438–444]. While the method is restricted to monotonically increasing contact areas, we show that it remains valid at the very beginning of the unloading phase as well. Based on this result, it is possible to derive closed form solutions following the classical procedure of functional formulations of viscoelasticity: (1) the identification of the indentation creep function, which is the indentation response to a Heaviside load; and (2) a convolution integral of the load history over the indentation creep function. This is shown here for a trapezoidal loading by a conical indenter on three linear isotropic viscoelastic materials with deviator creep: the 3-parameter Maxwell model, the 4-parameter Kelvin–Voigt model and the 5-parameter combined Kelvin–Voigt–Maxwell model. For these models, we derive closed form solutions that can be employed for the back-analysis of indentation results from the loading and holding period and for the definition of unloading time criteria that ensure that viscous effects are negligible in the unloading response.
© 2005 Elsevier Ltd. All rights reserved.

Keywords: Indentation; Conical indenter; Linear viscoelasticity; Creep; Unloading

1. Introduction

The aim of indentation analysis is to link indentation data, typically an indentation force vs. indentation depth curve, *P–h*, to meaningful mechanical properties of the indented material. It is common practice to condense the indentation data into two quantities, the hardness H and the indentation modulus M, which

are related to measured indentation data, namely the maximum indentation force $P_{\max}$, the initial slope (or indentation stiffness) S of the unloading curve, and the projected contact area A_c by

$$H \stackrel{\text{def}}{=} \frac{P_{\max}}{A_c} \tag{1}$$

$$S = \left. \frac{dP}{dh} \right|_{h=h_{\max}} \stackrel{\text{def}}{=} \frac{2}{\sqrt{\pi}} M \sqrt{A_c} \tag{2}$$

Traditionally, for metals, the hardness H was early on recognized to relate to strength properties of the indented material (Brinell, 1901; Tabor, 1951; Cheng and Cheng, 2004). The investigation of the link between the unloading slope S and the elasticity properties of the indented material is more recent, requiring depth sensing indentation techniques that provide a continuous record of the P–h curve during loading and unloading in an indentation test (Tabor, 1951; Doerner and Nix, 1986; Oliver and Pharr, 1992; Bulychev, 1999). Application of such techniques in indentation analysis confirmed the link provided by classical contact mechanic solutions (Hertz, 1882; Boussinesq, 1885; Love, 1939; Galin, 1961; Sneddon, 1965; Borodich and Keer, 2004) between the indentation modulus and the elasticity properties of the indented material. For instance, for an isotropic linear elastic (or elastoplastic) material indented by a rigid cone:

$$M = \frac{E}{1 - v^2} \tag{3}$$

where E is the Young modulus and v the Poisson's ratio. Several refinements to relation (2), which is also known as Bulychev–Alekhin–Shorshorov equation, or in short BASh-formula (Bulychev et al., 1975), have been proposed (for recent reviews see Cheng and Cheng (2004) and Oliver and Pharr (2004)). It is generally agreed today that combining accurate indentation data ($P_{\max}$, S, A_c) and relations (1) and (2) is a convenient way to extract intrinsic mechanical properties of materials that can be described by *time independent* constitutive relations.

The time dependence of the constitutive relations complicates indentation analysis. This is readily understood from a typical load-controlled indentation test, which consists of a loading, a holding, and an unloading phase (see Fig. 1). The load applied on the indenter is increased during the loading phase, kept constant at its maximum value during the holding phase, and decreased during the unloading phase. What is then observed for a wide range of materials, ranging from polymers to natural composite materials, is an increase of the indendation depth h during the holding phase (i.e. under constant load), which leads to an
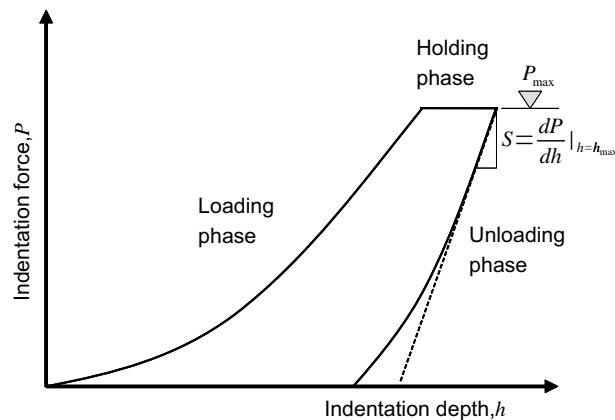

Fig. 1. A typical indentation force vs. indentation depth curve from an experimental indentation test.

increase in the contact area A_c and a decrease in the hardness (1) with time. Moreover, the time dependence of the constitutive behavior of the indented material may also affect the loading and unloading parts, when the time scales of loading and unloading interfere with the characteristic time scales of the time dependent material behavior. At very slow unloading rates, it is even possible to observe a negative initial unloading slope, $S < 0$! For this case, the BASh formula (2) would predict a negative indentation modulus M, which is obviously not admissible. In fact, experimental indentation results show that the unloading stiffness S can be overestimated if the holding phase is too short (Chudoba and Richter, 2001) or if the unloading phase is too long (Feng and Ngan, 2002). Of course, the question remains 'how fast the unloading phase?' should be and 'how long the holding phase?'—or more generally, how to account in indentation analysis for viscous phenomena and eventually relate indentation data to meaningful viscous material properties. This is in short the focus of this paper, to derive analytical contact solutions for trapezoidal load histories in conical indentation on a halfspace composed of a linear viscoelastic material that can be described by three deviator creep models: the 3-parameter Maxwell deviator creep model, the 4-parameter Kelvin–Voigt deviator creep model, and a combined 5-parameter Maxwell–Kelvin–Voigt deviator creep model. The analytical solutions are validated with finite element solutions where available and applied to indentation analysis of a microindentation test on a white cement paste.

2. Viscoelastic punch analysis

Most viscoelastic indentation solutions originate from the method of functional equations developed for linear viscoelastic contact problems by Radok (1957) and completed by Lee and Radok (1960). The method of functional equations consists in solving the viscoelastic problem from the elastic solution by replacing the elastic moduli with their corresponding viscoelastic operators. The method of functional equations can be seen as an extension of the Laplace transform method, as formulated by Lee (1955). The Laplace transform method consists in eliminating the explicit time dependence of the viscoelastic problem by applying the Laplace transform to the time dependent moduli and to solve the corresponding elasticity problem in the Laplace domain. The Laplace method, however, is restricted to boundary value problems, in which the displacement and stress boundary conditions are fixed in time. This is generally not the case in indentation problems (except for the flat punch problem), in which the contact area changes with time; hence changing a part of the stress boundary outside the contact area into a displacement boundary inside the contact area, and vice versa. This drawback of the Laplace transform was lifted by Radok (1957) and Lee and Radok (1960), who introduced and developed the method of functional equations, valid for linear viscoelastic problems with time dependent boundary conditions. Once the method of functional equations applied, if the boundary conditions are not explicitly expressed within the set of equations describing the contact problem, the use of the Laplace transform is valid, as a mere mathematical tool without physical meaning: in this specific case, the method of functional equations can be equated with the Laplace transform method. For indentation problems, the method of functional equations remains valid as long as the contact area (or, equivalently for viscoelastic materials, the penetration depth) increases monotonically (Lee and Radok, 1960). The restriction of the method to monotonically increasing contact area has haunted many researchers in the 1960s (e.g. solution for spherical indentation by Hunter (1960)) and was finally removed by Ting (1966), who developed implicit equations for the general case of indentation in any linear viscoelastic material by any axisymmetric indenter, and for any load history. But it is a challenge to employ Ting's implicit formulation, except for a few very specific load histories, indenter shapes and material behaviors. A similar remark can be made about the implicit solution procedure suggested by Galanov (1982) requiring for the solution a method of successive approximations. This may explain why Radok's method of functional equations is still attractive today, as testify some very recent analytical solutions for a Kelvin–Voigt material for flat punch indentation (Cheng et al., 2000) and for spherical indentation (Cheng et al., 2005).

Surprisingly, except for some ad-hoc solutions which are based on an empirical approach without solving the viscoelastic problem at a material level (e.g. Fischer-Cripps, 2004), and the very recent solution for a Kelvin–Voigt material by Cheng and Cheng (2005), we could not find closed form solutions for conical indentation, which is the reference indenter shape for most sharp indenters (Berkovich, Cube Corner, etc.) used in indentation testing. Furthermore, most existing solutions are restricted to the two simplest linear viscoelastic models (the Maxwell model (Feng and Ngan, 2002) or the 4-parameter Kelvin–Voigt model (Cheng et al., 2000; Cheng et al., 2005; Delafargue and Ulm, 2004)) which are too restrictive to capture the different viscoelastic phenomena that occur in real materials. Finally, due to the employment of the method of functional equations and its restriction to monotonically increasing contact areas, most solutions cannot address the question how viscous phenomena affect the initial unloading slope and hence the extracted elasticity properties. This motivated the developments presented below. We derive closed form solutions for different linear viscoelastic models for relevant load histories using the method of functional equations and show that this method remains valid to calculate the initial unloading slope.

2.1. Problem formulation

The problem we consider is the indentation of a rigid cone (half-angle θ) in a linear viscoelastic material (Fig. 2). The indentation test is load-controlled and follows a trapezoidal load history (see Fig. 1) defined by

$$P(t) = P_{\max} \mathcal{F}(t); \quad \mathcal{F}(t) = \begin{cases} t/\tau_L & \text{for } 0 \leqslant t \leqslant \tau_L \\ 1 & \text{for } \tau_L \leqslant t \leqslant \tau_L + \tau_H \\ (\tau_L + \tau_H + \tau_U - t)/\tau_U & \text{for } \tau_L + \tau_H \leqslant t \leqslant \tau_L + \tau_H + \tau_U \end{cases} \tag{4}$$

where $P_{\max}$ is the maximum indentation force, $\mathcal{F}(t)$ is the normalized load history, and τ_L, τ_H and τ_U define the durations of the loading, holding and unloading phases, respectively.

For any linear isotropic viscoelastic material, the constitutive relations can be derived from:

$$\sum_{i=0}^{i=I_1} p_i^d \frac{\partial^i}{\partial t^i} \boldsymbol{\sigma}^d(t) = \sum_{i=0}^{i=I_2} q_i^d \frac{\partial^i}{\partial t^i} 2\boldsymbol{\varepsilon}^d(t) \tag{5a}$$

$$\sum_{i=0}^{i=J_1} p_i^v \frac{\partial^i}{\partial t^i} \boldsymbol{\sigma}^v(t) = \sum_{i=0}^{i=J_2} q_i^v \frac{\partial^i}{\partial t^i} 3\boldsymbol{\varepsilon}^v(t) \tag{5b}$$
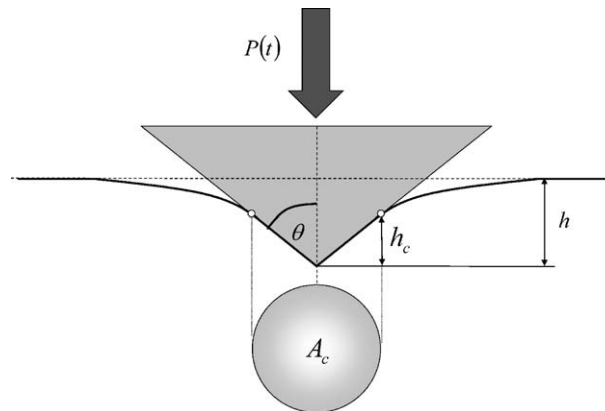

Fig. 2. Schematic of rigid conical indentation test: h is the indentation depth, h_c is the contact height, and A_c is the projected contact area.

where $\boldsymbol{\sigma}^{\mathrm{d}}$ and $\boldsymbol{\sigma}^{\mathrm{v}}$ are respectively the deviator and volumetric parts of the second order stress tensor $\boldsymbol{\sigma} = \boldsymbol{\sigma}^{\mathrm{d}} + \boldsymbol{\sigma}^{\mathrm{v}}$; $\boldsymbol{\varepsilon}^{\mathrm{d}}$ and $\boldsymbol{\varepsilon}^{\mathrm{v}}$ stand for the deviator and volumetric parts of the strain tensor $\boldsymbol{\varepsilon} = \boldsymbol{\varepsilon}^{\mathrm{d}} + \boldsymbol{\varepsilon}^{\mathrm{v}}$; and p_i^{d}, q_i^{d}, p_i^{v}, q_i^{v} are constants that describe the linear viscoelastic behavior. For instance, a purely elastic material of shear modulus G_0 and bulk modulus K_0 (or equivalently Young's modulus E_0 and Poisson's ratio v_0) is defined in (5) by $I_1 = I_2 = J_1 = J_2 = 0$ and:

$$G_0 = \frac{q_0^{\mathrm{d}}}{p_0^{\mathrm{d}}} = \frac{E_0}{2(1 + v_0)} \tag{6a}$$

$$K_0 = \frac{q_0^{\mathrm{v}}}{p_0^{\mathrm{v}}} = \frac{E_0}{3(1 - 2v_0)} \tag{6b}$$

If we note that a derivation in the time domain is equivalent to a multiplication by s in the Laplace domain, the great advantage of the general representation (5) of linear viscoelastic constitutive equations is that it allows for a straightforward representation in the Laplace domain:

$$\left(\sum_{i=0}^{i=I_1} p_i^{\mathrm{d}} s^i \right) \widehat{\boldsymbol{\sigma}^{\mathrm{d}}(s)} = \left(\sum_{i=0}^{i=I_2} q_i^{\mathrm{d}} s^i \right) 2 \widehat{\boldsymbol{\varepsilon}^{\mathrm{d}}(s)} \tag{7a}$$

$$\left(\sum_{i=0}^{i=J_1} p_i^{\mathrm{v}} s^i \right) \widehat{\boldsymbol{\sigma}^{\mathrm{v}}(s)} = \left(\sum_{i=0}^{i=J_2} q_i^{\mathrm{v}} s^i \right) 3 \widehat{\boldsymbol{\varepsilon}^{\mathrm{v}}(s)} \tag{7b}$$

where $\widehat{\boldsymbol{\sigma}^{\mathrm{d}}(s)}$, $\widehat{\boldsymbol{\sigma}^{\mathrm{v}}(s)}$, $\widehat{\boldsymbol{\varepsilon}^{\mathrm{d}}(s)}$, $\widehat{\boldsymbol{\varepsilon}^{\mathrm{v}}(s)}$ denote the Laplace transforms of $\boldsymbol{\sigma}^d(t)$, $\boldsymbol{\sigma}^{\mathrm{v}}(t)$, $\boldsymbol{\varepsilon}^{\mathrm{d}}(t)$, $\boldsymbol{\varepsilon}^{\mathrm{v}}(t)$. Relations (7) are particularly convenient to determine creep or relaxation functions employed in functional formulations of linear viscoelastic materials:

$$\boldsymbol{\varepsilon}(t) = \int_0^t \mathbb{C}(t - \tau) : \frac{\mathrm{d}}{\mathrm{d}\tau} \boldsymbol{\sigma}(\tau) \mathrm{d}\tau \tag{8a}$$

$$\boldsymbol{\sigma}(t) = \int_0^t \mathbb{R}(t - \tau) : \frac{\mathrm{d}}{\mathrm{d}\tau} \boldsymbol{\varepsilon}(\tau) \mathrm{d}\tau \tag{8b}$$

where $\mathbb{C}(t)$ and $\mathbb{R}(t)$ are the fourth order tensors of creep and relaxation functions of the material, which are related in the Laplace space by

$$\left(s \widehat{\mathbb{C}(s)} \right)^{-1} = s \widehat{\mathbb{R}(s)} \tag{9}$$

By way of illustration (but also because we will need them below), we consider the three linear isotropic deviator creep models displayed in Fig. 3. The elasticity in the models is defined by the instantaneous bulk and shear moduli K_0 and G_0 which are related to the other instantaneous material parameters and to the instantaneous indentation modulus by

$$\left\{ \begin{array}{l} E_0 = \frac{9K_0 G_0}{3K_0 + G_0} \\ v_0 = \frac{3K_0 - 2G_0}{6K_0 + 2G_0} \end{array} \right\} \Longleftrightarrow M_0 = 4G_0 \frac{3K_0 + G_0}{3K_0 + 4G_0} \tag{10}$$

In return, the viscous material response is defined by different creep and relaxation functions, that are readily obtained from (5) and (7):

1. The 3-parameter Maxwell deviator creep model (Fig. 3a) is obtained by introducing a Maxwell unit of viscosity η_{M} into the shear behavior. The expression of the viscous evolution law in the time domain reads:

$$2\dot{\boldsymbol{\varepsilon}}^{\mathrm{d}}(t) = \frac{\dot{\boldsymbol{\sigma}}^{\mathrm{d}}(t)}{G_0} + \frac{\boldsymbol{\sigma}^{\mathrm{d}}(t)}{\eta_{\mathrm{M}}} \tag{11}$$
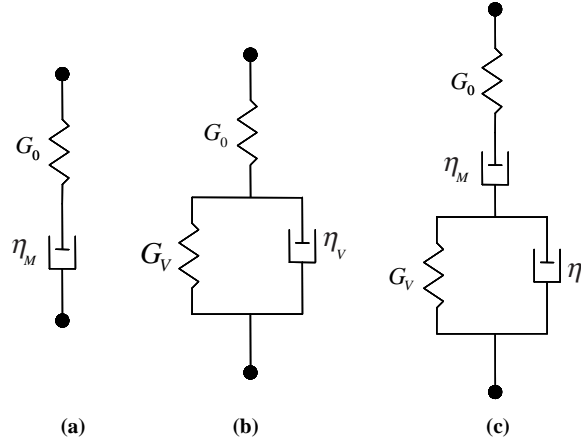
Fig. 3. Linear viscoelastic deviator creep models considered in this study: (a) the 3-parameter Maxwell model; (b) the 4-parameter Kelvin–Voigt model; (c) the 5-parameter combined Kelvin–Voigt–Maxwell model.

Then, expressing (11) in the Laplace domain allows one to derive the shear constitutive equation in the Laplace domain:

$$
\begin{aligned}
2\widehat{\varepsilon^{\mathrm{d}}(s)} &= \frac{\widehat{\sigma^{\mathrm{d}}(s)}}{G_0} + \frac{\widehat{\sigma^{\mathrm{d}}(s)}}{s\eta_{\mathrm{M}}} \\
&\Downarrow \\
\widehat{G(s)} &= \left(\frac{1}{G_0} + \frac{1}{s\eta_{\mathrm{M}}} \right)^{-1}
\end{aligned}
\tag{12}
$$

Using standard Laplace tables (e.g. Nixon, 1965) allows one to translate the shear creep function $(s\widehat{G(s)})^{-1}$, respectively the shear relaxation function $\widehat{G(s)}/s$, from the Laplace domain back into the time domain:

$$
\widehat{C^{\mathrm{d}}(s)} = \left(s\widehat{G(s)} \right)^{-1} \rightarrow C^{\mathrm{d}}(t) = \frac{1}{G_0} + \frac{t}{\eta_{\mathrm{M}}}
\tag{13a}
$$

$$
\widehat{R^{\mathrm{d}}(s)} = \frac{\widehat{G(s)}}{s} \rightarrow R^{\mathrm{d}}(t) = G_0 \mathrm{e}^{-\frac{G_0 t}{\eta_{\mathrm{M}}}}
\tag{13b}
$$

2. The 4-parameter Kelvin–Voigt deviator creep model (Fig. 3b) is obtained by introducing into the shear behavior a Kelvin–Voigt unit, i.e. a spring of stiffness G_{V} in parallel with a dashpot of viscosity η_{V}. This model can be defined as well by its delayed shear stiffness $G_\infty = (1/G_0 + 1/G_{\mathrm{V}})^{-1}$. The viscous evolution law reads:

$$
G_0 G_{\mathrm{V}} 2\varepsilon^{\mathrm{d}}(t) + G_0 \eta_{\mathrm{V}} 2\dot{\varepsilon}^{\mathrm{d}}(t) = (G_0 + G_{\mathrm{V}})\sigma^{\mathrm{d}}(t) + \eta_{\mathrm{V}} \dot{\sigma}^{\mathrm{d}}(t)
\tag{14}
$$

whence the shear constitutive equation in the Laplace domain:

$$
\begin{aligned}
2\widehat{\varepsilon^{\mathrm{d}}(s)} &= \frac{\widehat{\sigma^{\mathrm{d}}(s)}}{G_0} + \frac{\widehat{\sigma^{\mathrm{d}}(s)}}{G_{\mathrm{V}}+s\eta_{\mathrm{V}}} \\
&\Downarrow \\
\widehat{G(s)} &= \left(\frac{1}{G_0} + \frac{1}{G_{\mathrm{V}}+s\eta_{\mathrm{V}}} \right)^{-1}
\end{aligned}
\tag{15}
$$

and the shear relaxation and shear creep functions in the time domain:

$$
\widehat{C^{\mathrm{d}}(s)} = \left(s\widehat{G(s)} \right)^{-1} \rightarrow C^{\mathrm{d}}(t) = \frac{1}{G_0} + \frac{1}{G_{\mathrm{V}}}\left(1 - \mathrm{e}^{-\frac{G_{\mathrm{V}} t}{\eta_{\mathrm{V}}}} \right)
\tag{16a}
$$

$$
\widehat{R^{\mathrm{d}}(s)} = \frac{\widehat{G(s)}}{s} \rightarrow R^{\mathrm{d}}(t) = G_0 - \frac{G_0^2}{G_0 + G_{\mathrm{V}}}\left(1 - \mathrm{e}^{-\frac{(G_0 + G_{\mathrm{V}})t}{\eta_{\mathrm{V}}}} \right)
\tag{16b}
$$

3. A combination in series of the Kelvin–Voigt unit with the Maxwell unit (Fig. 3c) yields a 5-parameter deviator creep model for which the viscous deformation is given by

$$G_0\eta_V\eta_M 2\ddot{\boldsymbol{\varepsilon}}^d(t) + G_0 G_V\eta_M 2\dot{\boldsymbol{\varepsilon}}^d(t) = \eta_M\eta_V\ddot{\boldsymbol{\sigma}}^d(t) + (G_0\eta_V + G_0\eta_M + G_V\eta_M)\dot{\boldsymbol{\sigma}}^d(t) + G_0 G_V\boldsymbol{\sigma}^d(t) \quad (17)$$

The shear constitutive equation is readily obtained from:

$$\widehat{\boldsymbol{\varepsilon}^d(s)} = \frac{\widehat{\boldsymbol{\sigma}^d(s)}}{2G_0} + \frac{\widehat{\boldsymbol{\sigma}^d(s)}}{2(G_V + s\eta_V)} + \frac{\widehat{\boldsymbol{\sigma}^d(s)}}{2s\eta_M}$$
$$\Downarrow$$
$$\widehat{G(s)} = \left(\frac{1}{G_0} + \frac{1}{s\eta_M} + \frac{1}{G_V + s\eta_V}\right)^{-1} \quad (18)$$

Whence in the time domain:

$$\widehat{C^d(s)} = (s\widehat{G(s)})^{-1} \rightarrow C^d(t) = \frac{1}{G_0} + \frac{1}{G_V}\left(1 - e^{-\frac{G_V}{\eta_V}t}\right) + \frac{t}{\eta_M} \quad (19)$$

(The expression of the relaxation function is somewhat lengthy, and is omitted here).

Consider now a conical indentation test on a linear homogeneous viscoelastic halfspace. The dependent quantity of interest, the indentation depth h, depends on time t, the load history parameters (P_{max}, τ_L, τ_H, τ_U) defined by (4), the elastic properties (K_0, G_0 or E_0, v_0), the viscous properties (G_V, η_V, η_M, ...), and the indenter geometry (which in the case of conical indentation reduces to the half-apex angle θ). A straightforward application of dimensional analysis (or more precisely the Pi-theorem) allows us to define the relevant solution invariants:

$$\frac{E_0 h^2(t)}{P_{max}} = \Pi\left(\frac{t}{\tau_L}, \frac{\tau_H}{\tau_L}, \frac{\tau_U}{\tau_L}, v_0, \frac{G_V}{E_0}, \frac{\eta_V}{E_0 t}, \frac{\eta_M}{E_0 t}, \dots, \theta\right) \quad (20)$$

For an elastic material, relation (20) reduces to the classical Galin–Sneddon solution (Galin, 1961; Sneddon, 1965):

$$\frac{E_0 h^2(t)}{P_{max}} = \frac{\pi}{2}\frac{1 - v_0^2}{\tan\theta}\mathscr{F}(t) \Longleftrightarrow h^2(t) = \frac{\pi}{2\tan\theta}\frac{P(t)}{M_0} \quad (21)$$

where $\mathscr{F}(t)$ is the load-time history defined by (4). The elastic solution motivates us to seek for dimensionless solutions of the viscoelastic problem in the form:

$$y(t) = \frac{2}{\pi}\frac{M_0 h^2(t)}{P_{max}}4\tan\theta \quad (22)$$

where M_0 is the instantaneous indentation modulus defined by (10). Furthermore, for any linear viscoelastic material, as long as the contact area monotonically increases, i.e. during the loading and holding phase, the contact height to indentation depth ratio (see Fig. 2) is constant and equal to the elastic solution $h_c/h = 2/\pi$, so that $A_c(t)/h^2(t) = 4/\pi\tan^2\theta$ (Cheng and Cheng, 2004). This shows that $y(t)$ is close to a multiplying constant equal to $M_0/H(t)$ multiplied by the normalized load history:

$$y(t) = 2\cot\theta\frac{M_0}{H(t)}\begin{cases} t/\tau_L & \text{for } 0 \leqslant t \leqslant \tau_L \\ 1 & \text{for } \tau_L \leqslant t \leqslant \tau_L + \tau_H \end{cases} \quad (23)$$

where $H(t) = P(t)/A_c(t)$ is the time dependent hardness.

2.2. Response to a step load: indentation creep function

We start with the viscoelastic response to a step load defined by a Heaviside step function of the form:

$$P(t) = P_{\max} \mathscr{F}(t); \mathscr{F}(t) \equiv \mathscr{H}(t) = \begin{cases} 0 & \text{for } t < 0 \\ 1 & \text{for } t \geqslant 0 \end{cases} \tag{24}$$

For a linear isotropic elastic behavior of the half-space the response is given by the Galin–Sneddon solution (21). Based on the results of Radok and Lee (Radok, 1957; Lee and Radok, 1960), the method of functional equations allows one to obtain the viscoelastic solution from (21) by replacing the elastic constants by the Laplace transform of their corresponding viscoelastic operators:

$$\widehat{h^2(s)} = \frac{\pi}{2 \tan \theta} \frac{\widehat{P(s)}}{\widehat{M(s)}} \tag{25}$$

where $\widehat{h^2(s)}$ and $\widehat{P(s)}$ are the Laplace transforms of $h^2(t)$ and $P(t)$, while $\widehat{M(s)}$ is the Laplace transform of the differential operators associated with the now time dependent plane-stress modulus. Hence analogously to (3) and (10):

$$\widehat{M(s)} = \frac{\widehat{E(s)}}{1 - \left(\widehat{v(s)}\right)^2} = 4\widehat{G(s)} \frac{3\widehat{K(s)} + \widehat{G(s)}}{3\widehat{K(s)} + 4\widehat{G(s)}} \tag{26}$$

Note that the application of the method of functional equations to (21) and (25) implies that the contact height to indentation depth ratio is fixed, by definition, to a constant value $h_c/h = 2/\pi$. Finally, if we note that the Laplace transform $\widehat{P(s)}$ of the Heaviside load function (24) reads:

$$P(t) = P_{\max} \mathscr{H}(t) \Longleftrightarrow \widehat{P(s)} = \frac{P_{\max}}{s} \tag{27}$$

we obtain the following response to a step load in the Laplace domain:

$$\widehat{h^2(s)} = \frac{\pi}{2 \tan \theta} \frac{P_{\max}}{s\widehat{M(s)}} \tag{28}$$

or equivalently in terms of the invariant (22) which we denote for a step load by Y

$$\widehat{Y(s)} = \frac{2}{\pi} \frac{M_0 \widehat{h^2(s)}}{P_{\max}} 4 \tan \theta = 4 \frac{M_0}{s\widehat{M(s)}} \tag{29}$$

Hence, once $\widehat{M(s)}$ is specified, relation (29) allows one to determine the step load response in the Laplace domain and standard Laplace tables enable then to translate the response from the Laplace domain into the time domain, i.e. $\widehat{Y(s)} \rightarrow Y(t)$.

By way of application, let us consider the three viscoelastic models displayed in Fig. 3. Since the creep models are all deviatoric, the bulk modulus is time independent and its Laplace transform coincides with its value in the time domain:

$$\widehat{K(s)} = K_0 \tag{30}$$

In return, the shear relaxation functions are given by (12), (15) and (18), respectively. In more detail:

1. *3-parameter Maxwell model*: Use of (12) and (30) in (26) yields:

$$\widehat{M(s)} = 4G_0 \frac{\eta_M s(3K_0 G_0 + s\eta_M(3K_0 + G_0))}{(s\eta_M + G_0)(3K_0 G_0 + s\eta_M(3K_0 + 4G_0))} \tag{31}$$

Then, substituting (31) in (29) gives the step load response in the Laplace domain:

$$\frac{\widehat{Y(s)}}{4M_0} = \frac{K_0 + G_0}{4K_0 G_0}\frac{1}{s} + \frac{1}{4\eta_{\mathrm{M}}}\frac{1}{s^2} - \frac{G_0\eta_{\mathrm{M}}}{4K_0}\frac{1}{3K_0 G_0 + (3K_0 + G_0)\eta_{\mathrm{M}}s} \tag{32}$$

and application of standard Laplace tables yields the expression in the time domain:

$$Y(t) = 4 + \frac{M_0}{\eta_{\mathrm{M}}}t + \frac{(1 - 2v_0)^2}{(1 - v_0^2)}\left(1 - \mathrm{e}^{-\frac{E_0 t}{3\eta_{\mathrm{M}}}}\right) \tag{33}$$

The step load response is governed in time by a linear term and an exponential one. While the relaxation term vanishes as time increases, the linear term remains and leads to an indentation response without asymptote which is scaled, for large times, by $h(t) \propto \sqrt{t}$ (similar to a diffusion phenomenon!). We also note that the slope of the linear term is linked with the time constant of the exponential term by a proportionality factor $3(1 - v_0^2)$. In other words, the Maxwell model introduces only one time constant.

2. *4-parameter Kelvin–Voigt model*: Use of (15) and (30) in (26) yields:

$$\widehat{M(s)} = 4G_0\frac{(G_{\mathrm{V}} + s\eta_{\mathrm{V}})(3K_0(G_0 + G_{\mathrm{V}} + s\eta_{\mathrm{V}}) + G_0(G_{\mathrm{V}} + s\eta_{\mathrm{V}}))}{(G_0 + G_{\mathrm{V}} + s\eta_{\mathrm{V}})(3K_0(G_0 + G_{\mathrm{V}} + s\eta_{\mathrm{V}}) + 4G_0(G_{\mathrm{V}} + s\eta_{\mathrm{V}}))} \tag{34}$$

Then, a substitution of (34) in (29) gives the expression of the step load response in the Laplace domain, which after backtransformation in the time domain becomes:

$$Y(t) = 4 + \frac{M_0}{G_{\mathrm{V}}}\left(1 - \mathrm{e}^{-\frac{G_{\mathrm{V}}t}{\eta_{\mathrm{V}}}}\right) + \frac{M_0(1 - 2v_0)^2}{E_0 + 3G_{\mathrm{V}}}\left(1 - \mathrm{e}^{-\frac{(E_0 + 3G_{\mathrm{V}})t}{3\eta_{\mathrm{V}}}}\right) \tag{35}$$

The step load response of the Kelvin–Voigt model is characterized by two exponential terms defined by two distinct time scales, which from the material relaxation and creep functions (16) can be identified as the characteristic creep time $\eta_{\mathrm{V}}/G_{\mathrm{V}}$ and a time $\eta_{\mathrm{V}}/(E_0/3 + G_{\mathrm{V}})$ resulting from a coupling between the instantaneous elastic properties and both the material relaxation and creep times. This shows that indentation creep activates, at a material level, both creep and relaxation phenomena. Both exponential terms vanish as time t increases, so that the step load response tends to an asymptotic value:

$$\lim_{t\to\infty} Y(t) = 4 + \frac{M_0}{G_{\mathrm{V}}} + \frac{M_0(1 - 2v_0)^2}{E_0 + 3G_{\mathrm{V}}} \tag{36}$$

3. *5-parameter combined Kelvin–Voigt–Maxwell model*: Using (18) and (30) in (26) and substituting the result in (29) yields the step load response in the Laplace domain, which equates to the following response in the time domain:

$$Y(t) = \frac{5 - 4v_0}{1 - v_0^2} + \frac{M_0}{\eta_{\mathrm{M}}}t + \frac{M_0}{G_{\mathrm{V}}}\left(1 - \mathrm{e}^{-\frac{t}{T_2}}\right) - \frac{(1 - 2v_0)^2}{(1 - v_0^2)\left(\frac{1}{T_1} - \frac{1}{T_3}\right)}\left[\left(\frac{1}{T_2} - \frac{1}{T_3}\right)\mathrm{e}^{-\frac{t}{T_3}} + \left(\frac{1}{T_1} - \frac{1}{T_2}\right)\mathrm{e}^{-\frac{t}{T_1}}\right] \tag{37}$$

where the time constants $T_1 < T_2 < T_3$ are given by

$$\begin{cases} T_1 = \dfrac{6\eta_{\mathrm{M}}\eta_{\mathrm{V}}}{E_0(\eta_{\mathrm{V}} + \eta_{\mathrm{M}}) + 3\eta_{\mathrm{M}}G_{\mathrm{V}} + \sqrt{E_0^2(\eta_{\mathrm{V}} + \eta_{\mathrm{M}})^2 + 6E_0\eta_{\mathrm{M}}G_{\mathrm{V}}(\eta_{\mathrm{M}} - \eta_{\mathrm{V}}) + 9\eta_{\mathrm{M}}^2 G_{\mathrm{V}}^2}} \\[4mm] T_2 = \dfrac{\eta_{\mathrm{V}}}{G_{\mathrm{V}}} \\[4mm] T_3 = \dfrac{6\eta_{\mathrm{M}}\eta_{\mathrm{V}}}{E_0(\eta_{\mathrm{V}} + \eta_{\mathrm{M}}) + 3\eta_{\mathrm{M}}G_{\mathrm{V}} - \sqrt{E_0^2(\eta_{\mathrm{V}} + \eta_{\mathrm{M}})^2 + 6E_0\eta_{\mathrm{M}}G_{\mathrm{V}}(\eta_{\mathrm{M}} - \eta_{\mathrm{V}}) + 9\eta_{\mathrm{M}}^2 G_{\mathrm{V}}^2}} \end{cases} \tag{38}$$

The step load response of the model is governed in time by a linear term and three exponential terms of three different time scales (T_1, T_2, T_3). T_2 can be identified as the characteristic creep time of the Kelvin–Voigt unit. T_1 and T_3 are combinations of the elastic properties of the material and the relaxation and creep times of the Maxwell and Kelvin–Voigt models. For $\eta_M \gg \eta_V$, the characteristic times simplify:

$$\begin{cases} T_1 \simeq T_1^a = \dfrac{3\eta_V}{E_0 + 3G_V} \\[2mm] T_2 = \dfrac{\eta_V}{G_V} \\[2mm] T_3 \simeq T_3^a = \dfrac{(E_0 + 3G_V)\eta_M}{E_0 G_V} \end{cases} \tag{39}$$

and $T_3^a \gg T_2$ and $T_3^a \gg T_1^a$.

While the exponential terms in (37) vanish for large values of t, the linear time term remains: $Y(t)$ has no asymptote.

Without difficulty we verify that the step load responses (33), (35) and (37) reduce to the instantaneous elastic solution for $t = 0$:

$$Y(0) = 4$$

Finally, we should note that expression (25) holds for any monotonically increasing load. Hence, if we introduce the step load response $\widehat{Y(s)}$ in (25) we obtain after re-arrangement:

$$\widehat{y(s)} = \frac{4}{P_{\max}} \frac{M_0}{\widehat{M(s)}} \widehat{P(s)} = \frac{4}{P_{\max}} \frac{M_0}{s\widehat{M(s)}} s\widehat{P(s)} = \frac{1}{P_{\max}} \widehat{Y(s)}\, s\, \widehat{P(s)} \tag{40}$$

Recalling now that a derivation in the time domain is equivalent to a multiplication by s in the Laplace domain, and that a convolution product between two functions in the time domain is equivalent, in the Laplace domain, to a multiplication between their Laplace transforms, we obtain the following general dimensionless solution in the time domain for any monotonically increasing load case:

$$y(t) = \frac{2}{\pi} \frac{M_0 h^2(t)}{P_{\max}} 4\tan\theta = \frac{1}{P_{\max}} \int_0^t Y(t-\tau)\frac{\mathrm{d}}{\mathrm{d}\tau}P(\tau)\mathrm{d}\tau \tag{41}$$

Hence, by analogy of (41) with the classical functional formulation of linear viscoelasticity (8a), we identify the fundamental step load solution $Y(t)$ as the indentation creep function. In other words, once $Y(t)$ is known, the dimensionless indentation response $y(t)$ can be determined for any monotonically increasing load history.

2.3. Application to a trapezoidal load history: loading and holding phase

By way of application, we consider the loading and the holding phases of the trapezoidal load history given by (4). During loading, $P(t) = P_L(t) = P_{\max}t/\tau_L$. Use in (41) yields:

$$y_L(t) = \frac{1}{P_{\max}} \int_0^t Y(t-\tau)\frac{\mathrm{d}}{\mathrm{d}\tau}P_L(\tau)\mathrm{d}\tau = \frac{1}{\tau_L} \int_0^t Y(t-\tau)\mathrm{d}\tau \quad \text{for } t \leqslant \tau_L \tag{42}$$

On the other hand, in order to access the indentation response for the holding phase, the integral in (41) needs to be evaluated for both the loading phase $P(t) = P_{\max}t/\tau_L$ and the holding phase $P(t) = P_H(t) = P_{\max}$. Hence:

$$y_H(t) = \frac{1}{P_{\max}} \int_0^{\tau_L} Y(t-\tau)\frac{\mathrm{d}}{\mathrm{d}\tau}P_L(\tau)\mathrm{d}\tau + \frac{1}{P_{\max}} \int_{\tau_L}^t Y(t-\tau)\frac{\mathrm{d}}{\mathrm{d}\tau}P_H(\tau)\mathrm{d}\tau = \frac{1}{\tau_L} \int_0^{\tau_L} Y(t-\tau)\mathrm{d}\tau + 0 \tag{43}$$

That is:

$$y_H(t) = \frac{1}{\tau_L} \int_0^{\tau_L} Y(t - \tau) d\tau \quad \text{for } \tau_L \leqslant t \leqslant \tau_L + \tau_H \tag{44}$$

By way of illustration, we re-consider the three deviatoric creep models, for which the indentation creep functions are given by (33), (35) and (37) respectively. Use in (42) and (44) yields the dimensionless responses:

1. *3-parameter Maxwell model*: Use of (33) in (42) and (44) yields for the loading phase:

$$y_L(t) = \frac{1}{\tau_L} \left(\frac{5 - 4v_0}{1 - v_0^2} t + \frac{M_0}{\eta_M} \frac{t^2}{2} - \left(\frac{1 - 2v_0}{1 - v_0^2} \right)^2 \frac{3\eta_M}{M_0} \left(1 - e^{-\frac{E_0 t}{3\eta_M}} \right) \right) \tag{45}$$

and for the holding phase:

$$y_H(t) = \frac{5 - 4v_0}{1 - v_0^2} + \frac{M_0}{\eta_M} \left(t - \frac{\tau_L}{2} \right) - \left(\frac{1 - 2v_0}{1 - v_0^2} \right)^2 \frac{3\eta_M}{M_0 \tau_L} \left(e^{\frac{E_0 \tau_L}{3\eta_M}} - 1 \right) e^{-\frac{E_0 t}{3\eta_M}} \tag{46}$$

As in the step load response (33), we find that the holding response is characterized by a linear and an exponential term.

2. *4-parameter Kelvin–Voigt model*: Substitution of (35) in (42) and (44) yields the loading response:

$$y_L(t) = \frac{1}{\tau_L} \left(\left(4 + \frac{M_0}{G_V} + (1 - 2v_0)^2 \frac{M_0}{E_0 + 3G_V} \right) t - \frac{\eta_V M_0}{G_V^2} \left(1 - e^{-\frac{G_V}{\eta_V} t} \right) - \frac{3\eta_V M_0 (1 - 2v_0)^2}{(E_0 + 3G_V)^2} \left(1 - e^{-\frac{E_0 + 3G_V}{3\eta_V} t} \right) \right) \tag{47}$$

and the holding response:

$$y_H(t) = \left(4 + \frac{M_0}{G_V} + \frac{M_0 (1 - 2v_0)^2}{E_0 + 3G_V} + \frac{\eta_v M_0}{G_V^2 \tau_L} \left(1 - e^{\frac{G_V \tau_L}{\eta_V}} \right) e^{-\frac{G_V t}{\eta_V}} + \frac{3\eta_V M_0 (1 - 2v_0)^2}{(E_0 + 3G_V)^2 \tau_L} \left(1 - e^{\frac{(E_0 + 3G_V)\tau_L}{3\eta_V}} \right) e^{-\frac{(E_0 + 3G_V)t}{3\eta_V}} \right) \tag{48}$$

The holding response of the Kelvin–Voigt model displays the two exponential terms of the indentation creep function (35), associated respectively with material creep (characteristic creep time η_V/G_V) and a combination of creep and relaxation time of the material (characteristic time $\eta_V/(E_0/3 + G_V)$). Both exponential terms vanish as time t increases, so that the holding response tends to the asymptotic value (36):

$$\lim_{t \to \infty} y_H(t) = \lim_{t \to \infty} Y(t) \tag{49}$$

3. *5-parameter combined Kelvin–Voigt–Maxwell model*: The loading and holding responses of the combined Kelvin–Voigt–Maxwell model are obtained from substituting (37) in (42) and (44). This yields after evaluation of the integrals for the loading phase:

$$y_L(t) = \frac{1}{\tau_L} \left(\frac{5 - 4v_0}{1 - v_0^2} t + \frac{M_0}{G_V} \left(t - T_2 \left(1 - e^{-\frac{t}{T_2}} \right) \right) + \frac{M_0 t^2}{2\eta_M} - \frac{(1 - 2v_0)^2}{(1 - v_0^2)\left(\frac{1}{T_1} - \frac{1}{T_3} \right)} \left[\left(\frac{T_3}{T_2} - 1 \right) \left(1 - e^{-\frac{t}{T_3}} \right) \right.$$

$$\left. + \left(1 - \frac{T_1}{T_2} \right) \left(1 - e^{-\frac{t}{T_1}} \right) \right] \right) \tag{50}$$

and for the holding phase:

$$y_H(t) = \left(\frac{5 - 4v_0}{1 - v_0^2} + \frac{M_0}{G_V} - \frac{M_0 T_2}{G_V \tau_L} e^{-\frac{t}{T_2}} \left(e^{\frac{\tau_L}{T_2}} - 1 \right) + \frac{M_0}{\eta_M} \left(t - \frac{\tau_L}{2} \right) - \frac{(1 - 2v_0)^2}{\tau_L (1 - v_0^2) \left(\frac{1}{T_1} - \frac{1}{T_3} \right)} \right.$$

$$\left. \times \left[\left(\frac{T_3}{T_2} - 1 \right) e^{-\frac{t}{T_3}} \left(e^{\frac{\tau_L}{T_3}} - 1 \right) + \left(1 - \frac{T_1}{T_2} \right) e^{-\frac{t}{T_1}} \left(e^{\frac{\tau_L}{T_1}} - 1 \right) \right] \right) \tag{51}$$

We identify in the holding response (51) the time functions characterizing the indentation creep function (37) of the combined Kelvin–Voigt–Maxwell model: the linear non-asymptotic time term and the three exponential terms defined by the characteristic times (38) and (39). Like (37), the holding response $y_H(t)$ has no asymptote.

3. Initial unloading slope

3.1. Limits of the method of functional equations for unloading

The method of functional equations is restricted to the case of monotonically increasing contact areas, which is obviously not the case upon unloading. This is readily seen from the P–h curves displayed in Fig. 4 which compare the indentation response for the 4-parameter Kelvin–Voigt deviator creep model obtained from the method of functional equations with the results of a finite element simulation performed by Cheng and Cheng (2004). The load function considered is a symmetric triangular loading–unloading ramp, defined by

$$P(t) = P_{max} \mathscr{F}(t); \quad \mathscr{F}(t) = \begin{cases} t/\tau_L & \text{for } t \leqslant \tau_L \\ 2 - t/\tau_L & \text{for } \tau_L \leqslant t \leqslant 2\tau_L \end{cases} \tag{52}$$
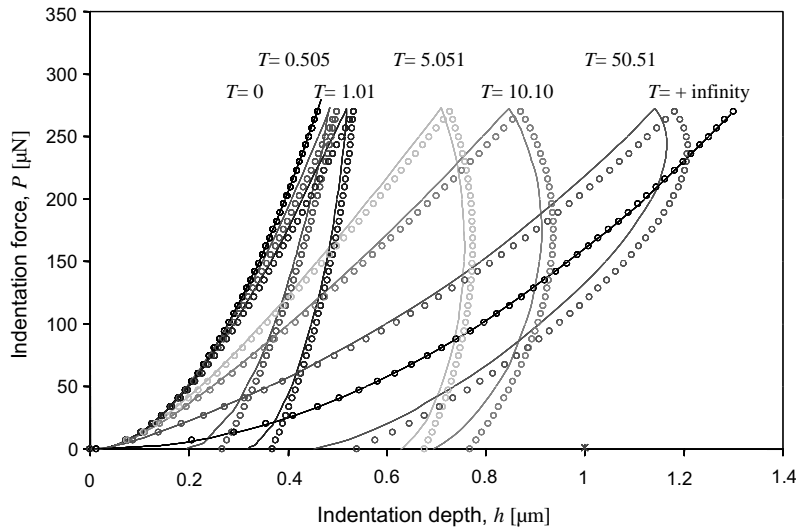

Fig. 4. Validation of viscoelastic solution: Comparison of P–h curves from finite element solution (solid lines) of Cheng and Cheng (2004) and our analytical solution (dotted lines). The comparison is made for the Kelvin–Voigt deviator creep model and symmetric triangular loading–unloading for different dimensionless loading–unloading times, $\mathscr{T} = \tau_L (G_0 + G_V)/\eta_V$.

In the simulations $P_{max} = 270\,\mu N$, and the loading time is varied in a way that the time invariant $\mathscr{T} = \tau_L(G_0 + G_V)/\eta_V$ spans a large range of values, from $\mathscr{T} = 0^+$ (infinitely fast loading and unloading phases) to $\mathscr{T} \to \infty$ (infinitely slow loading and unloading phases). The four model input values for the simulations are: $G_0 = 234.60$ MPa, $K_0 = 687.62$ MPa, $G_V = 25.78$ MPa and $\eta_V = 257.78$ MPa s; which correspond to an instantaneous indentation modulus of $M_0 = 718.34$ MPa, a Young's modulus of $E_0 = 631.93$ MPa, and a Poisson's ratio of $v_0 = 0.35$. These are all the parameters requested to calculate the loading response from (47). The results of the comparison of the numerical solution and our analytical solution are displayed in Fig. 4. Remarkably, but not surprisingly, our analytical solution (47) compares very well with the finite element results for the loading phase, which validates our solution. Nevertheless, we notice that the analytical solution tends to slightly overestimate the displacements by roughly 3%. The reason for this (small but existing) overestimation needs to be sought for in the elastic Galin–Sneddon solution (21), on which the viscoelastic solution is based (i.e. relation (25)). In fact, as discussed by many (Hay et al., 1999; Cheng and Cheng, 2004; Oliver and Pharr, 2004), the Galin–Sneddon solution is first order in nature, as it neglects the elastic radial contraction of the surface in contact with the indenter. To compensate for this effect, it is common practice to multiply the Galin–Sneddon solution by a correction factor; here $\beta \simeq 1.03$. In this case, we obtain a perfect agreement of our solution with the FE-results, which validates our solution for the loading phase.

Analogously, we attempted to derive the response for the unloading phase using the method of functional equations, by substituting the load–unloading history (52) together with the indentation creep function (35) in (41):

$$y_U(t) = \frac{1}{\tau_L} \int_0^{\tau_L} Y(t-\tau)\mathrm{d}\,\tau - \frac{1}{\tau_L} \int_{\tau_L}^t Y(t-\tau)\mathrm{d}\tau \tag{53}$$

This gives:

$$
\begin{aligned}
y_U(t) = &\left(4 + \frac{M_0}{G_V} - \frac{\eta_v M_0}{\tau_L G_V^2} e^{-\frac{G_V t}{\eta_V}}\left(e^{\frac{\tau_L G_V}{\eta_V}} - 1\right) + (1-2v_0)^2 \frac{M_0}{E_0 + 3G_V} - \frac{(1-2v_0)^2}{1-v_0^2}\frac{3M_0\eta_V}{(E_0+3G_V)^2\tau_L} e^{-\frac{(E_0+3G_V)t}{3\eta_V}}\right. \\
&\times \left(e^{\frac{\tau_L(E_0+3G_V)}{3\eta_V}} - 1\right) - 4\frac{t-(\tau_L+\tau_H)}{\tau_L} - \frac{M_0}{G_V}\frac{t-(\tau_L+\tau_H)}{\tau_L} + \frac{\eta_V M_0}{\tau_L G_V^2}\left(1 - e^{-\frac{G_V(t-(\tau_L+\tau_H))}{\eta_V}}\right) \\
&\left. -(1-2v_0)^2\frac{M_0}{E_0+3G_V}\frac{t-(\tau_L+\tau_H)}{\tau_L} + (1-2v_e)^2\frac{3\eta_V M_0}{\tau_L(E_0+3G_V)^2}\left(1 - e^{-\frac{(E_0+3G_V)(t-(\tau_L+\tau_H))}{3\eta_V}}\right)\right)
\end{aligned}
\tag{54}
$$

Fig. 4 also shows a comparison of the numerical results with the unloading response obtained from the method of functional equations (54). It appears that the analytical solution performs very well at the beginning of the unloading part, while the displacements deviate from the FE-solution at the end of the unloading part. This shows the limitation of the analytical solution: as predicted by Lee and Radok (1960), the use of the principle of superposition, during the unloading phase, leads to negative pressures at the surface of the half-space, which is not admissible, and which manifests itself in an overestimation of the displacements. Hence, the analytical solutions are only valid as long as the contact area monotonically increases, i.e. during the loading and the holding phases, and possibly for parts of the unloading phase. In fact, for specific load cases (here, for $\mathscr{T} = 5.051, 10.10$ and 50.51), the P–h curves show a 'bulge': the contact area is still increasing whereas the load is already decreasing. In such cases, the analytical solution remains valid during the first part of the unloading, since the penetration depth (and consequently the contact area) is still increasing whereas the load starts decreasing. This is illustrated in Fig. 5 which displays the contact area vs. time, for $\mathscr{T} = 10.10$, together with the load history, in a normalized form. Our analytical solution is
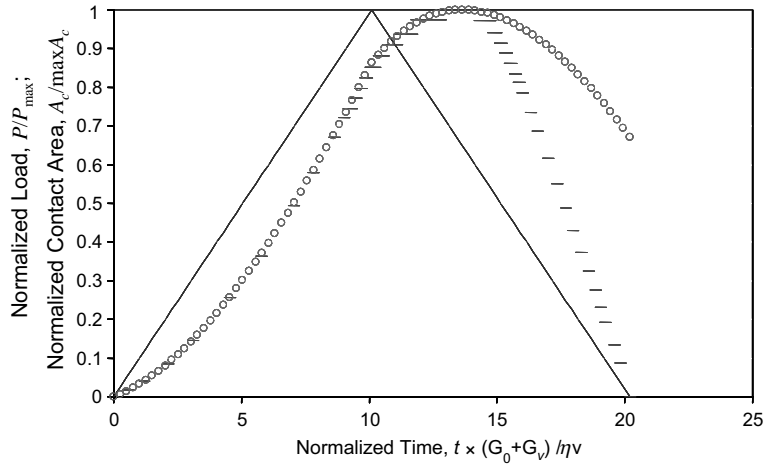
Fig. 5. Indentation load (solid line) and contact area development in conical indentation of a Kelvin–Voigt material for $\mathcal{T} = \tau_L(G_0 + G_V)/\eta_V = 10.10$ (curve with 'bulge' in Fig. 4): as long as the contact area increases, the analytical solution (dotted line) obtained from the method of functional equations with $h/h_c = 2/\pi$ perfectly agrees with the finite element results of Cheng and Cheng (2004) (dashed line). Once the contact area decreases, the analytical solution diverges dramatically from the numerical one, showing the limit of the method of functional equations.

obtained from (47) and (54), which yields the indentation depth history $h(t)$. Then noting that $h_c(t)/h(t) = 2/\pi$ as long as the contact area increases allows us to determine the contact area, $A_c(t) = 4/\pi h^2(t)\tan^2\theta$. As expected, as long as the contact area increases, which here extends into the unloading phase ('bulge'), our analytical results are in excellent agreement with the numerical solution by Cheng and Cheng (2004). But, as soon as the contact area decreases, our solution diverges dramatically from the numerical one, which shows that the elastic solution $h_c/h = 2/\pi$ is no more valid: the solution does not provide a link between the penetration depth and the contact depth, respectively the contact area. From a practical point of view, we disregard curves with a bulge, since the measured contact stiffness S is obviously distorted by viscous phenomena and cannot be linked directly to instantaneous elastic properties. But for other load cases for which the P–h curves show no bulge (here, in Fig. 4, for $\mathcal{T} = 0.505, 1.01$), the penetration depth and the contact area decrease from the beginning of the unloading. In such cases, it is to be expected that our analytical solutions which are based on the method of functional equations should no more be valid. Nevertheless, we show in the next section that the method of functional equations remains valid to calculate the initial unloading slope of the P–h curve.

3.2. The effect of viscous properties on the contact stiffness

We are interested in quantifying the effects of viscous properties on the initial unloading slope or contact stiffness S, obtained after a loading and holding period from the P–h curve:

$$S = \frac{dP}{dh}\bigg|_{t=(\tau_L+\tau_H)^+} = \frac{\dot{P}(t = (\tau_L + \tau_H)^+)}{\dot{h}(t = (\tau_L + \tau_H)^+)} \tag{55}$$

Recalling (22), we express the indentation rate $\dot{h}$ in function of $y(t)$ and $\dot{y}(t)$:

$$\dot{h}(t) = \frac{\dot{y}(t)}{4\sqrt{y(t)}}\sqrt{\frac{\pi}{2}\frac{P_{max}}{M_0 \tan\theta}} \tag{56}$$

Furthermore, in the case of a trapezoidal loading, the unloading rate is $\dot{P} = -P_{\max}/\tau_{\mathrm{U}}$, so that the contact stiffness (55) becomes:

$$S = \left.\frac{\mathrm{d}P}{\mathrm{d}h}\right|_{t=(\tau_{\mathrm{L}}+\tau_{\mathrm{H}})^{+}} = -\frac{4\sqrt{y(t=(\tau_{\mathrm{L}}+\tau_{\mathrm{H}})^{+})}}{\dot{y}(t=(\tau_{\mathrm{L}}+\tau_{\mathrm{H}})^{+})\tau_{\mathrm{U}}}\sqrt{\frac{2P_{\max}M_0\tan\theta}{\pi}} \tag{57}$$

or equivalently, recalling that $A_{\mathrm{c}}(t)/h^2(t) = 4/\pi\tan^2\theta$ in any conical indentation test into a linear viscoelastic material, during which the contact area monotonically increases (Cheng and Cheng, 2004), i.e. during the loading and holding phases; and which holds, by continuity, for the onset of unloading $t=(\tau_{\mathrm{L}}+\tau_{\mathrm{H}})^{+}$:

$$S = \left.\frac{\mathrm{d}P}{\mathrm{d}h}\right|_{t=(\tau_{\mathrm{L}}+\tau_{\mathrm{H}})^{+}} = S_0\left(\frac{-4}{\dot{y}(t=(\tau_{\mathrm{L}}+\tau_{\mathrm{H}})^{+})\tau_{\mathrm{U}}}\right) \tag{58}$$

where S_0 is the time independent expression of the BASh formula (2):

$$S_0 = \frac{2}{\sqrt{\pi}}M_0\sqrt{A_{\mathrm{c}}(t=(\tau_{\mathrm{L}}+\tau_{\mathrm{H}})^{+})} \tag{59}$$

with A_{c} the projected contact area. Hence, viscous effects affect the actual contact stiffness through the dimensionless factor $-4/(\dot{y}\tau_{\mathrm{U}})$ in (58). To evaluate this factor, we need to determine $y_{\mathrm{U}}(t)$ for the unloading phase. This cannot be achieved with confidence from the method of functional equations (i.e. relation (41)), without giving proof that the method of functional equations actually applies to the initial part of the indentation unloading phase. The proof, which is somewhat lengthy, but of critical importance, is given in Appendix A. It is based on the equivalence of Ting's general (but implicit) solution which is valid for any loading history (Ting, 1966), and the (explicit) method of functional equations, for $t=(\tau_{\mathrm{L}}+\tau_{\mathrm{H}})^{+}$. Based on this proof, it is possible to evaluate the viscous effects on the contact stiffness S. For the considered trapezoidal loading, application of the load history (4) in (41) yields the unloading response $y_{\mathrm{U}}(t)$, and its time derivative evaluated at $(\tau_{\mathrm{L}}+\tau_{\mathrm{H}})^{+}$ is obtained:

$$\dot{y}_{\mathrm{U}}(t=(\tau_{\mathrm{L}}+\tau_{\mathrm{H}})^{+}) = \frac{\mathrm{d}}{\mathrm{d}t}\left(\frac{1}{\tau_{\mathrm{L}}}\int_0^{\tau_{\mathrm{L}}}Y(t-\tau)\mathrm{d}\tau - \frac{1}{\tau_{\mathrm{U}}}\int_{\tau_{\mathrm{L}}+\tau_{\mathrm{H}}}^{t}Y(t-\tau)\mathrm{d}\tau\right)_{t=(\tau_{\mathrm{L}}+\tau_{\mathrm{H}})^{+}} \tag{60}$$

Use of (60) in (58) allows us to evaluate the deviation of the measurable contact stiffness S from the instantaneous contact stiffness S_0. For the three deviator creep models considered earlier, it is possible to show that, for an infinitely fast unloading (i.e. for $\tau_{\mathrm{U}} \to 0^{+}$), $S_0/S = 1$. This shows that, theoretically, by unloading 'fast enough', it should be possible to measure the correct instantaneous contact stiffness S_0.

By way of application of (60), we re-consider the three deviatoric creep models, for which the indentation creep functions are given by (33), (35) and (37) respectively:

1. *3-parameter Maxwell model*: $Y(t)$ is given by (33), and application of (60) in (58) yields:

$$\frac{S_0}{S} = -\frac{\dot{y}(t=(\tau_{\mathrm{L}}+\tau_{\mathrm{H}})^{+})\tau_{\mathrm{U}}}{4} = 1 - \frac{M_0\tau_{\mathrm{U}}}{4\eta_{\mathrm{M}}} - \frac{(1-2v_0)^2\tau_{\mathrm{U}}}{4(1-v_0^2)\tau_{\mathrm{L}}}\mathrm{e}^{-\frac{E_0\tau_{\mathrm{H}}}{3\eta_{\mathrm{M}}}}\left(1-\mathrm{e}^{-\frac{E_0\tau_{\mathrm{L}}}{3\eta_{\mathrm{M}}}}\right) \tag{61}$$

For $\tau_{\mathrm{U}} > 0$, we observe as expected a viscous stiffening of the measurable contact stiffness, $S \geqslant S_0$. Hence, to reduce this error in the estimation of the instantaneous elasticity properties from (2) (resp. (59)) the second term on the r.h.s. of (61) must be much smaller than unity. This allows us to derive the following criterion for the unloading time:

$$\tau_{\mathrm{U}} \ll 4\left[\frac{M_0}{\eta_{\mathrm{M}}} + \frac{(1-2v_0)^2}{(1-v_0^2)\tau_{\mathrm{L}}}\mathrm{e}^{-\frac{E_0\tau_{\mathrm{H}}}{3\eta_{\mathrm{M}}}}\left(1-\mathrm{e}^{-\frac{E_0\tau_{\mathrm{L}}}{3\eta_{\mathrm{M}}}}\right)\right]^{-1} \Rightarrow S \simeq S_0 \tag{62}$$

An interesting observation is that the unloading time criterion of the Maxwell model depends on both the loading and the holding times, τ_L and τ_H, in addition to the viscoelastic properties of the indented material (E_0, v_0, η_M) and to the related characteristic time of the Maxwell, η_M/E_0. Relation (62) highlights the role of both loading and holding phases. The greater τ_L and τ_H, the longer the unloading phase can be. Nevertheless, even for infinitely long loading and holding phases, the unloading time must be much smaller than the relaxation time of the Maxwell unit, so that the contact stiffness S can be used with confidence to determine the instantaneous elasticity properties.

2. *4-parameter Kelvin–Voigt model*: Use of (35) in (60) yields:

$$\frac{S_0}{S} = 1 - \frac{\tau_U M_0}{4\tau_L G_V} e^{-\frac{G_V \tau_H}{\eta_V}}\left(1 - e^{-\frac{G_V \tau_L}{\eta_V}}\right) - \frac{\tau_U M_0 (1 - 2v_0)^2}{4\tau_L (E_0 + 3G_V)} e^{-\frac{(E_0 + 3G_V)\tau_H}{3\eta_V}}\left(1 - e^{-\frac{(E_0 + 3G_V)\tau_L}{3\eta_V}}\right) \tag{63}$$

Hence, $S \simeq S_0$ requires here:

$$\tau_U \ll 4\tau_L \left[\frac{M_0}{G_V} e^{-\frac{G_V \tau_H}{\eta_V}}\left(1 - e^{-\frac{G_V \tau_L}{\eta_V}}\right) + \frac{M_0 (1 - 2v_0)^2}{(E_0 + 3G_V)} e^{-\frac{(E_0 + 3G_V)\tau_H}{3\eta_V}}\left(1 - e^{-\frac{(E_0 + 3G_V)\tau_L}{3\eta_V}}\right)\right]^{-1} \tag{64}$$

The unloading time criterion of the Kelvin–Voigt model depends on both the loading and the holding times, τ_L and τ_H, in addition to the viscoelastic properties of the indented material (E_0, v_0, G_V, η_V) and to the related characteristic times of the Kelvin–Voigt model, η_V/G_V and $\eta_V/(E_0/3 + G_V)$. The greater τ_L and τ_H, the longer the unloading phase can be. In other words, the closer the indentation response during loading and holding is to its asymptotic value (49), the less do viscous effects affect the initial unloading response.

3. *5-parameter combined Kelvin–Voigt–Maxwell model*: Use of (37) in (60) yields:

$$\frac{S_0}{S} = 1 - \frac{M_0 \tau_U}{4\eta_M} - \frac{\tau_U M_0}{4\tau_L G_V} e^{-\frac{\tau_H}{T_2}}\left(1 - e^{\frac{\tau_L}{T_2}}\right)$$
$$- \frac{(1 - 2v_0)^2 \tau_U}{4\tau_L (1 - v_0^2)\left(\frac{1}{T_1} - \frac{1}{T_3}\right)}\left(\left(\frac{1}{T_2} - \frac{1}{T_3}\right)e^{-\frac{\tau_H}{T_3}}\left(1 - e^{-\frac{\tau_L}{T_3}}\right) + \left(\frac{1}{T_1} - \frac{1}{T_2}\right)e^{-\frac{\tau_H}{T_1}}\left(1 - e^{-\frac{\tau_L}{T_1}}\right)\right) \tag{65}$$

Hence, the unloading time criterion which limits viscous phenomena to affect the elastic unloading response, reads here:

$$\tau_U \ll 4\left[\frac{M_0}{\eta_M} + \frac{M_0}{\tau_L G_V} e^{-\frac{\tau_H}{T_2}}\left(1 - e^{\frac{\tau_L}{T_2}}\right) + \frac{(1 - 2v_0)^2}{\tau_L (1 - v_0^2)\left(\frac{1}{T_1} - \frac{1}{T_3}\right)}\left(\left(\frac{1}{T_2} - \frac{1}{T_3}\right)e^{-\frac{\tau_H}{T_3}}\left(1 - e^{-\frac{\tau_L}{T_3}}\right)\right.\right.$$
$$\left.\left. + \left(\frac{1}{T_1} - \frac{1}{T_2}\right)e^{-\frac{\tau_H}{T_1}}\left(1 - e^{-\frac{\tau_L}{T_1}}\right)\right)\right]^{-1} \tag{66}$$

where the time constants (T_1, T_2, T_3) are given by (38) and (39). Once again, the greater τ_L and τ_H, the longer the unloading phase can be. Moreover, even for infinitely long loading and holding phases, the unloading time must be much smaller than the relaxation time of the Maxwell unit.

4. Example of viscoelastic analysis of a microindentation on a white cement paste

By way of example, we consider a microindentation on a white cement paste. The indentation test was performed with the three-sided pyramidal Berkovich indenter, which is assimilated to a conical indenter of equivalent cone angle $\theta = 70.32°$. The load history is trapezoidal characterized by $P_{\max} = 1$ N, $\tau_L = 33.2$ s, $\tau_H = 149.7$ s and $\tau_U = 33.5$ s. We seek to identify the viscoelastic properties of the material from the

measured indentation data, $h(t)$. We will first assume that viscous phenomena have no influence on the measured contact stiffness ($S \simeq S_0$), and we will verify this assumption a posteriori. The input parameters are the instantaneous elastic properties, i.e. the indentation modulus M_0, which we determine from (2) in the conventional fashion, employing the Oliver and Pharr method (Oliver and Pharr, 1992) for contact area estimation, and the Poisson's ratio v_0, respectively the instantaneous elastic modulus E_0.

In order to identify which model fits best the data, we fit the different viscous model parameters of the three analytical models (46), (48) and (51) to the measured holding response of the indentation test. This fitting is performed with Matlab using a conventional non linear least-square method. The results are displayed in Fig. 6. The model parameters and the fitting errors are summarized in Table 1, together with the
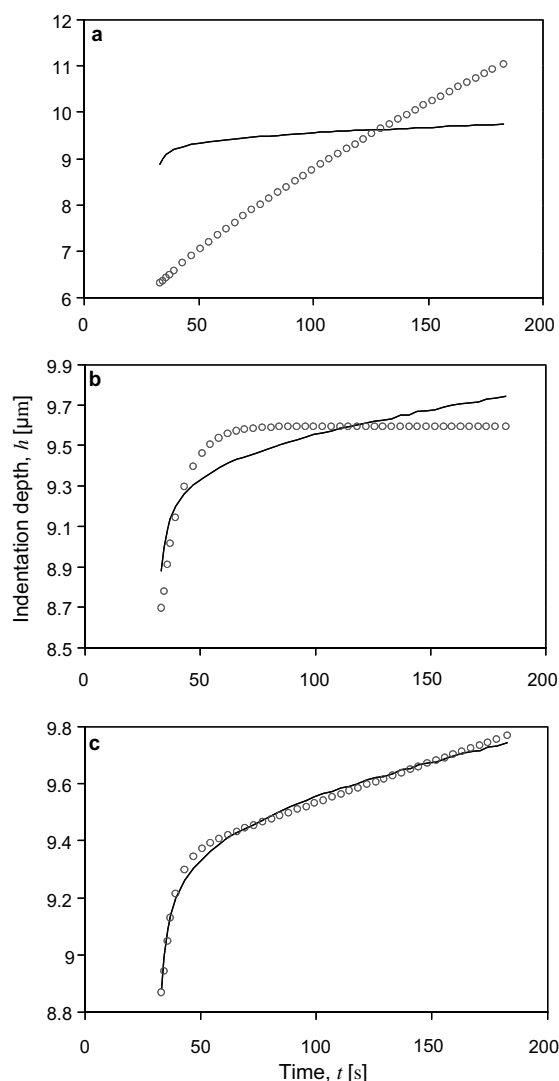

Fig. 6. Backanalysis of the holding response $h(t)$ of a Berkovich microindentation test on a white cement paste for three viscoelastic deviator creep models: (a) Maxwell model, (b) Kelvin–Voigt model, (c) combined Maxwell–Kelvin–Voigt model. Experimental results (solid line) and fitted model responses (dotted line).

Table 1
Viscoelastic properties extracted from the indentation holding phase

	Maxwell	Kelvin–Voigt	Combined
M_0 [GPa][a]	18.5	18.5	18.5
v_0 [1][b]	0.24	0.24	0.24
η_M [GPa s]	261.7	–	2579.6
G_V [GPa]	–	2.3	2.6
η_V [GPa s]	–	21.7	13.4
Fitting error[c] [1]	1895	12.2	0.47
S_0/S [1]	0.40	1.00	0.94

[a] The indentation modulus M_0 was determined from the contact stiffness S by assuming viscous effects negligible.
[b] The value of $v_0 = 0.24$ is the Poisson's ratio generally assumed for cement-based materials.
[c] The fitting error is estimated by the squared 2-norm of the residual of the least square fitting performed on the dimensionless variable y.

S_0/S-ratios determined from (61), (63) and (65), respectively. Not surprisingly, as the number of model parameters increases, the fitting error decreases:

1. *3-parameter Maxwell model*: Since this model has only one viscous degree of freedom (i.e. η_M), the depth at the beginning of the holding depends on the load history during the loading phase in (46), which explains the poor performance of the model (Fig. 6). A higher initial depth can only be obtained by decreasing η_M. However, decreasing η_M leads to an increase of the average slope of the depth-time curve during the holding phase, which yields a worse fit. Finally, the error one commits by considering the unloading response as quasi-instantaneous is significant; in fact, according to (61), the viscosity should go to infinity in order to ensure $S \simeq S_0$.
2. *4-parameter Kelvin–Voigt model*: While the model improves the prediction of the depth at the onset of the holding period (Fig. 6), it performs poorly during the holding period because of its asymptotic nature (36). On the other hand, the relatively short relaxation time $\eta_V/G_V = 9.4$ s ensures that there are little viscous phenomena involved in the initial unloading response, so that $S \simeq S_0$.
3. *5-parameter combined Kelvin–Voigt–Maxwell model*: In the fitting of the model, we assumed $\eta_M \gg \eta_V$ and considered the set of approximated time constants (39) instead of the set of exact ones (38). The assumption is readily verified from the values in Table 1. The model with its two viscous mechanisms

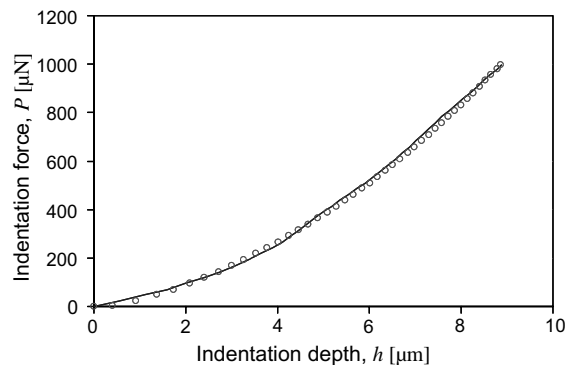Fig. 7. Validation of viscoelastic fitting procedure: The *P–h* curve of the loading phase calculated with viscoelastic parameters (dotted line) fitted for the loading phase for the combined Maxwell–Kelvin–Voigt model agrees very well with the experimental results (solid line).

associated with different time scales allows us to capture with high accuracy the features of the experimental indentation curve. Furthermore, using the values in (65), it is found that the relative error one commits by considering the measured contact stiffness S as the instantaneous stiffness S_0 is on the order of 6%. This small error justifies a posteriori the use of conventional methods for the extraction of the instantaneous modulus M_0. Finally, the viscous parameters were fitted for the holding period. It is interesting to check the relevance of the data for the loading period as well, by introducing the data into (50). The predicted loading response is displayed in Fig. 7, and agrees remarkably well with the experimental curve. This could mean that not only the holding phase, but as well the loading phase of the tested material is dominated by viscoelastic behavior, and in particular by the short-time Kelvin–Voigt unit having a relaxation time on the same order as the loading time. On the contrary, the long-term Maxwell unit having a relaxation time on the order of $\eta_M/M_0 = 139$ s affects little the loading response during $\tau_L = 33.2$ s.

5. Conclusions

The framework of viscoelastic indentation analysis presented in this paper is based on the method of functional equations, which is a powerful method to derive closed form solutions for any conventional indenter, loading history and any linear viscoelastic material whose time dependent properties can be expressed analytically in the Laplace domain. The method of functional equations, as defined initially by Lee and Radok (1960), is restricted to monotonically increasing contact areas. Nevertheless, we showed that it remains valid at the very beginning of the unloading phase as well. This is an important result, both theoretically and practically, as it allows one to quantify analytically the deviation of the measured initial unloading slope S from the instantaneous indentation stiffness S_0; and hence the effect of viscous properties on the indentation modulus. The method is simple and follows the classical procedure of functional formulations of viscoelasticity, namely (1) the identification of the indentation creep function, which is the indentation response to a Heaviside load; and (2) a convolution integral of the load history over the indentation creep function. The principles were illustrated for a trapezoidal loading by a conical indenter on three linear viscoelastic materials with deviator creep: the 3-parameter Maxwell deviator creep model, the 4-parameter Kelvin–Voigt deviator creep model and the 5-parameter combined Kelvin–Voigt–Maxwell deviator creep model. For these models, we derived closed form solutions that can be employed for the back-analysis of indentation results from the loading and holding period, and for the definition of unloading time criteria, which ensure that viscous effects are negligible in the unloading response. While derived here in the context of conical indentation, the same dimensionless solutions equally apply to other indenter geometries. Indeed, it suffices to appropriately adapt the dimensionless expression (22) to the indenter geometry. The application to microindentation data of a white cement paste showed how to employ the solutions; i.e. determination of the viscoelastic parameters from a fit of the holding response, and check of relevance of the fit for the loading period. Of course, the use of our solutions requires that the overall indentation response is dominated by a linear viscoelastic behavior, and that other effects such as plastic deformations are negligible.

Acknowledgement

Appendix A. Proof of relevance of method of functional equations for calculating the initial unloading slope

We show in this appendix that the method of functional equations used to calculate the response during the loading and holding phases still remains valid to calculate the initial unloading slope of the load-displacement curve. The proof is based on the results of Ting (1966), who succeeded in solving analytically, in an implicit form, the problem of the indentation of a linear viscoelastic half-space by a rigid axisymmetric indenter for a load case with any number of extrema.

A.1. Presentation of Ting's solution

We consider the case of a contact area monotonically increasing and then decreasing. Ting introduces in his solution several auxiliary functions and parameters:

- $a(t)$ is the radius of the contact area.
- t_m is the time at which $a(t)$ reaches its maximum.
- $t_1(t)$ is an auxiliary time, introduced for $t > t_m$. $t_1(t)$ is defined by: $a(t_1) = a(t)$ and $t_1(t) < t_m$.
- $\Psi(t)$ and $\Phi(t)$ are two material functions, defined from the relaxation functions of the material according to the following equations in the Laplace domain:

$$s\widehat{\Phi(s)} = \frac{\widehat{\lambda(s)} + 2\widehat{G(s)}}{2s\widehat{G(s)}(\widehat{\lambda(s)} + \widehat{G(s)})} \quad \text{and} \quad s\widehat{\Psi(s)} = \frac{1}{s\widehat{\Phi(s)}}$$

where $\widehat{\Psi(s)}$, $\widehat{\Phi(s)}$, $\widehat{\lambda(s)}$ and $\widehat{G(s)}$ are the Laplace transforms of $\Psi(t)$, $\Phi(t)$, $\lambda(t)$ and $G(t)$. $\lambda(t)$ and $G(t)$ are the relaxations functions of the Lame's coefficients.
- $h_e(t)$ is the penetration depth solution for an elastic material. For a circular conical indenter $h_e(t)$ can be expressed as follows: $h_e(t) = \frac{\pi}{2\tan(\alpha)} a(t)$.
- $P_e(t)$ is the solution for the load applied on the indenter for an elastic material. For a circular indenter $P_e(t)$ can be expressed as $cP_e(t) = \frac{\pi a^2(t)}{\tan(\alpha)} = \frac{4\tan(\alpha)}{\pi} h_e^2(t)$, where $c = \frac{1-\nu}{G}$.

With the above notations, Ting's solution of the considered viscoelastic problem has the following implicit form:

$$\begin{cases} h(t) = h_e(t) \\ P(t) = \int_{0^-}^{t} \Psi(t-\tau)\frac{\partial}{\partial\tau}(cP_e(\tau))d\tau \end{cases} \quad \text{for } 0 \leqslant t \leqslant t_m \tag{67}$$

$$\begin{cases} h(t) = h_e(t) - \int_{t_m}^{t} \Phi(t-\tau)\frac{\partial}{\partial\tau}\int_{t_1(\tau)}^{\tau}\Psi(\tau-\eta)\frac{\partial}{\partial\eta}h_e(\eta)d\eta\,d\tau \\ P(t) = \int_{0^-}^{t_1(t)}\Psi(t-\tau)\frac{\partial}{\partial\tau}(cP_e(\tau))d\tau \end{cases} \quad \text{for } t_m \leqslant t \tag{68}$$

A.2. Equivalence of Ting's solution and the method of functional equations

First of all, we have to check that the solution developed by Ting for $0 \leqslant t \leqslant t_m$ gives the same results as the method of functional equations. The problem of the circular conical indentation of an elastic material is governed by the equation:

$$h_e^2(t) = \frac{\pi}{2\tan(\alpha)}\frac{1-\nu^2}{E}P_e(t) \tag{69}$$

Therefore, the use of the method of functional equations allows us to assert that the problem of the circular indentation of a linear viscoelastic material, for $0 \leqslant t \leqslant t_m$, is governed in the Laplace domain by

$$\widehat{h^2(s)} = \frac{\pi}{2\tan(\alpha)} \frac{1 - \left(\widehat{v(s)}\right)^2}{\widehat{E(s)}} \widehat{P(s)} = \frac{\pi}{2\tan(\alpha)} \frac{\widehat{P(s)}}{\widehat{M(s)}} \tag{70}$$

where $\widehat{h^2(s)}$ and $\widehat{P(s)}$ are the Laplace transforms of respectively $h^2(t)$ and $P(t)$. $\widehat{v(s)}$ and $\widehat{E(s)}$ are the Laplace transforms of the differential operators associated with the viscoelastic Poisson's ratio and Young's modulus.

Ting's solution for the circular conical indentation of a linear viscoelastic material, for $0 \leqslant t \leqslant t_m$, can be rewritten as:

$$P(t) = \int_{0^-}^{t} \Psi(t - \tau) \frac{\partial}{\partial \tau} (cP_e(\tau)) \mathrm{d}\tau = \int_{0^-}^{t} \Psi(t - \tau) \frac{\partial}{\partial \tau} \left(\frac{4\tan(\alpha)}{\pi} h_e^2(\tau) \right) \mathrm{d}\tau$$

$$= \frac{4\tan(\alpha)}{\pi} \int_{0^-}^{t} \Psi(t - \tau) \frac{\partial}{\partial \tau} (h^2(\tau)) \mathrm{d}\tau \tag{71}$$

A derivation in the time domain is equivalent to a multiplication by s in the Laplace domain. A convolution product between two functions in the time domain is equivalent, in the Laplace domain, to a multiplication between their Laplace transforms. Therefore, Ting's solution can be rewritten in the Laplace domain as:

$$\widehat{P(s)} = \frac{4\tan(\alpha)}{\pi} \widehat{\Psi(s)} s \widehat{h^2(s)} \tag{72}$$

which yields:

$$\widehat{h^2(s)} = \frac{\pi}{4\tan(\alpha)} \frac{1}{s\widehat{\Psi(s)}} = \frac{\pi}{4\tan(\alpha)} s\widehat{\Phi(s)} \tag{73a}$$

$$= \frac{\pi}{8\tan(\alpha)} \frac{\widehat{\lambda(s)} + 2\widehat{G(s)}}{\widehat{G(s)}(\widehat{\lambda(s)} + \widehat{G(s)})} \tag{73b}$$

Finally, if we employ the elastic relations,

$$\lambda = E \frac{v}{(1+v)(1-2v)}; \quad G = \frac{E}{2(1+v)} \tag{74}$$

we have for a viscoelastic material:

$$\widehat{\lambda(s)} = \widehat{E(s)} \frac{\widehat{v(s)}}{(1 + \widehat{v(s)})(1 - 2\widehat{v(s)})} \tag{75a}$$

$$\widehat{G(s)} = \frac{\widehat{E(s)}}{2(1 + \widehat{v(s)})} \tag{75b}$$

Then, Eq. (73) yields:

$$\widehat{h^2(s)} = \frac{\pi}{2\tan(\alpha)} \frac{\widehat{P(s)}}{\widehat{M(s)}}; \quad \widehat{M(s)} = \frac{\widehat{E(s)}}{1 - (\widehat{v(s)})^2} \tag{76}$$

which is the same equation as (25). Therefore, for $0 \leqslant t \leqslant t_m$, Ting's solution and the method of functional equations are equivalent.

A.3. Calculation of the initial unloading slope

The initial slope of the unloading part of the load–displacement curve is given by $\left(\frac{\mathrm{d}P}{\mathrm{d}h}\right)_{t=t_{\mathrm{m}}^+} = \frac{\dot{P}(t_{\mathrm{m}}^+)}{\dot{h}(t_{\mathrm{m}}^+)}$. We want to check if Ting's solution for $0 \leqslant t \leqslant t_{\mathrm{m}}$, extended to $t = t_{\mathrm{m}}^+$, gives the same results as Ting's solution for $t_{\mathrm{m}} \leqslant t$. We assume that $\Psi(t)$ and $\Phi(t)$ are continuous and derivable on $[0, t]$, and that $P(t)$, $P_{\mathrm{e}}(t)$, $h(t)$ and $h_{\mathrm{e}}(t)$ are continuous on $[0, t]$ and derivable on $[0, t_{\mathrm{m}}[$ and $]t_{\mathrm{m}}, t]$. The proof will require the use of the following relationship, valid for any continuous and derivable function $f(x, y)$:

$$\frac{\mathrm{d}}{\mathrm{d}x} \int_0^x f(x, y)\mathrm{d}y = f(x, x) + \int_0^x \frac{\partial}{\partial x} f(x, y)\mathrm{d}y \tag{77}$$

Since we consider a load-controlled test, whatever the set of equation considered, $\dot{P}(t_{\mathrm{m}}^+)$ is a prescribed data. Therefore, $\dot{h}(t_{\mathrm{m}}^+)$ can be calculated from the set of Eq. (67) as well as from the set of Eq. (68). The calculation of the initial unloading slope from the set of Eq. (67) yields:

$$\dot{h}(t_{\mathrm{m}}^+) = \lim_{t \to t_{\mathrm{m}}^+} \dot{h}(t) = \dot{h}_{\mathrm{e}}(t_{\mathrm{m}}^+) \tag{78}$$

The use of the set of Eq. (68) leads to:

$$\dot{h}(t_{\mathrm{m}}^+) = \lim_{t \to t_{\mathrm{m}}^+} \left[\dot{h}_{\mathrm{e}}(t) - \frac{\mathrm{d}}{\mathrm{d}t} \left(\int_{t_{\mathrm{m}}^+}^t \Phi(t - \tau) \frac{\mathrm{d}}{\mathrm{d}\tau} \left(\int_{t_1(\tau)}^\tau \Psi(\tau - \eta) \frac{\mathrm{d}}{\mathrm{d}\eta} h_{\mathrm{e}}(\eta)\mathrm{d}\eta \right) \mathrm{d}\tau \right) \right] \tag{79}$$

Furthermore, by applying (77), we have:

$$\frac{\mathrm{d}}{\mathrm{d}t} \left(\int_{t_{\mathrm{m}}^+}^t \Phi(t - \tau) \frac{\mathrm{d}}{\mathrm{d}\tau} \left(\int_{t_1(\tau)}^\tau \Psi(\tau - \eta) \dot{h}_{\mathrm{e}}(\eta)\mathrm{d}\eta \right) \mathrm{d}\tau \right)$$

$$= \Phi(0) \frac{\mathrm{d}}{\mathrm{d}t} \left(\int_{t_1(t)}^t \Psi(t - \eta) \dot{h}_{\mathrm{e}}(\eta)\mathrm{d}\eta \right) + \int_{t_{\mathrm{m}}^+}^t \dot{\Phi}(t - \tau) \frac{\mathrm{d}}{\mathrm{d}\tau} \left(\int_{t_1(\tau)}^\tau \Psi(\tau - \eta) \dot{h}_{\mathrm{e}}(\eta)\mathrm{d}\eta \right) \mathrm{d}\tau \tag{80}$$

Since,

$$\lim_{t \to t_{\mathrm{m}}^+} \int_{t_{\mathrm{m}}^+}^t \dot{\Phi}(t - \tau) \frac{\mathrm{d}}{\mathrm{d}\tau} \left(\int_{t_1(\tau)}^\tau \Psi(\tau - \eta) \dot{h}_{\mathrm{e}}(\eta)\mathrm{d}\eta \right) \mathrm{d}\tau = 0 \tag{81}$$

we have:

$$\dot{h}(t_{\mathrm{m}}^+) = \dot{h}_{\mathrm{e}}(t_{\mathrm{m}}^+) - \Phi(0) \frac{\mathrm{d}}{\mathrm{d}t} \left(\int_{t_1(t)}^t \Psi(t - \eta) \dot{h}_{\mathrm{e}}(\eta)\mathrm{d}\eta \right)_{t=t_{\mathrm{m}}^+} \tag{82}$$

which can be decomposed into:

$$\dot{h}(t_{\mathrm{m}}^+) = \dot{h}_{\mathrm{e}}(t_{\mathrm{m}}^+) - \Phi(0) \frac{\mathrm{d}}{\mathrm{d}t} \left(\int_{t_{\mathrm{m}}^+}^t \Psi(t - \eta) \dot{h}_{\mathrm{e}}(\eta)\mathrm{d}\eta \right)_{t=t_{\mathrm{m}}^+} + \Phi(0) \frac{\mathrm{d}}{\mathrm{d}t} \left(\int_{t_{\mathrm{m}}^-}^{t_1(t)} \Psi(t - \eta) \dot{h}_{\mathrm{e}}(\eta)\mathrm{d}\eta \right)_{t=t_{\mathrm{m}}^+} \tag{83}$$

The application of (77) to the first integral term in (83) leads to:

$$\frac{\mathrm{d}}{\mathrm{d}t} \left(\int_{t_{\mathrm{m}}^+}^t \Psi(t - \eta) \dot{h}_{\mathrm{e}}(\eta)\mathrm{d}\eta \right)_{t=t_{\mathrm{m}}^+} = \lim_{t \to t_{\mathrm{m}}^+} \left[\Psi(0) \dot{h}_{\mathrm{e}}(t) + \left(\int_{t_{\mathrm{m}}^+}^t \dot{\Psi}(t - \eta) \dot{h}_{\mathrm{e}}(\eta)\mathrm{d}\eta \right) \right] = \Psi(0) \dot{h}_{\mathrm{e}}(t_{\mathrm{m}}^+) \tag{84}$$

The application of (77) to the second integral term in (83) leads to:

$$
\begin{aligned}
\frac{\mathrm{d}}{\mathrm{d}t}\left(\int_{t_\mathrm{m}^-}^{t_1(t)} \Psi(t-\eta)\dot{h}_\mathrm{e}(\eta)\mathrm{d}\eta\right)_{t=t_\mathrm{m}^+} &= \lim_{t\to t_\mathrm{m}^+}\frac{\mathrm{d}}{\mathrm{d}t}\left(\int_{t_\mathrm{m}^-}^{t_1(t)} \Psi(t-\eta)\dot{h}_\mathrm{e}(\eta)\mathrm{d}\eta\right) \\
&= \lim_{t\to t_\mathrm{m}^+}\left[\dot{t}_1(t)\frac{\mathrm{d}}{\mathrm{d}t_1}\left(\int_{t_\mathrm{m}^-}^{t_1(t)} \Psi(t-\eta)\dot{h}_\mathrm{e}(\eta)\mathrm{d}\eta\right)\right] \\
&= \dot{t}_1(t_\mathrm{m}^+)\lim_{t\to t_\mathrm{m}^+}\left[\frac{\mathrm{d}}{\mathrm{d}t_1}\left(\int_{t_\mathrm{m}^-}^{t_1(t)} \Psi(t-\eta)\dot{h}_\mathrm{e}(\eta)\mathrm{d}\eta\right)\right] \\
&= \dot{t}_1(t_\mathrm{m}^+)\lim_{t\to t_\mathrm{m}^+}\left[\Psi(t(t_1)-t_1)\dot{h}_\mathrm{e}(t_1)+\int_{t_\mathrm{m}^-}^{t_1(t)}\left(\dot{\Psi}(t-\eta)\dot{h}_\mathrm{e}(\eta)/\dot{t}_1(t)\right)\mathrm{d}\eta\right]
\end{aligned}
\tag{85}
$$

Since $\lim_{t\to t_\mathrm{m}^+}t_1(t)=t_\mathrm{m}^-$, we eventually have:

$$
\begin{aligned}
\frac{\mathrm{d}}{\mathrm{d}t}\left(\int_{t_\mathrm{m}^-}^{t_1(t)} \Psi(t-\eta)\dot{h}_\mathrm{e}(\eta)\mathrm{d}\eta\right)_{t=t_\mathrm{m}^+} &= \dot{t}_1(t_\mathrm{m}^+)\lim_{t_1\to t_\mathrm{m}^-}\left[\Psi(t(t_1)-t_1)\dot{h}_\mathrm{e}(t_1)+\int_{t_\mathrm{m}^-}^{t_1(t)}\left(\dot{\Psi}(t-\eta)\dot{h}_\mathrm{e}(\eta)/\dot{t}_1(t)\right)\mathrm{d}\eta\right] \\
&= \dot{t}_1(t_\mathrm{m}^+)\Psi(0)\dot{h}_\mathrm{e}(t_\mathrm{m}^-)
\end{aligned}
\tag{86}
$$

Finally, by using the set of Eq. (68), $\dot{h}(t_\mathrm{m}^+)$ can be expressed as follows:

$$
\dot{h}(t_\mathrm{m}^+) = \dot{h}_\mathrm{e}(t_\mathrm{m}^+) - \Phi(0)\Psi(0)[\dot{h}_\mathrm{e}(t_\mathrm{m}^+) - \dot{t}_1(t_\mathrm{m}^+)\dot{h}_\mathrm{e}(t_\mathrm{m}^-)]
\tag{87}
$$

We now come back to the definition of $t_1(t)$:

$$
a(t) = a(t_1(t))
\tag{88}
$$

which after derivation with respect to t can be rewritten as

$$
\dot{a}(t) = \dot{a}(t_1)\dot{t}_1(t)
\tag{89}
$$

which leads to:

$$
\lim_{t\to t_\mathrm{m}^+}\dot{a}(t) = \lim_{t\to t_\mathrm{m}^+}\dot{a}(t_1)\dot{t}_1(t)
\tag{90}
$$

and

$$
\dot{a}(t_\mathrm{m}^+) = \dot{a}(t_\mathrm{m}^-)\dot{t}_1(t_\mathrm{m}^+)
\tag{91}
$$

Since $h_\mathrm{e}(t)=g(a(t))$ where g is a derivable function, we have:

$$
\dot{h}_\mathrm{e}(t) = \dot{g}(a(t))\dot{a}(t)
\tag{92}
$$

and:

$$
\frac{\dot{h}_\mathrm{e}(t_\mathrm{m}^+)}{\dot{h}_\mathrm{e}(t_\mathrm{m}^-)} = \frac{\dot{g}(a(t_\mathrm{m}^+))\dot{a}(t_\mathrm{m}^+)}{\dot{g}(a(t_\mathrm{m}^-))\dot{a}(t_\mathrm{m}^-)}
\tag{93}
$$

Since $a(t)$ is a continuous function, we eventually find that:

$$
\frac{\dot{h}_\mathrm{e}(t_\mathrm{m}^+)}{\dot{h}_\mathrm{e}(t_\mathrm{m}^-)} = \frac{\dot{a}(t_\mathrm{m}^+)}{\dot{a}(t_\mathrm{m}^-)} = \dot{t}_1(t_\mathrm{m}^+)
\tag{94}
$$

Therefore, the calculation of the initial unloading slope by the use of the valid set of Eq. (68) leads to:

$$\dot{h}(t_{\mathrm{m}}^{+}) = \dot{h}_{\mathrm{e}}(t_{\mathrm{m}}^{+}) \tag{95}$$

which is equal to the result given by the set of Eq. (67). This proves that the method of functional equations can be applied to the calculation of the initial unloading slope.

References

Borodich, F.M., Keer, L.M., 2004. Contact problems and depth-sensing nanoindentation for frictionless and frictional boundary conditions. Int. J. Sol. Struct. 41, 2479–2499.

Boussinesq, J., 1885. Applications des potentiels a l'etude de l'equilibre et du mouvement des solides elastiques. Gauthier-Villars.

Brinell, J.A., 1901. Memoire sur les epreuves a bille en acier. In: Proceedings of the Congres International des Methodes d'Essai des Materiaux de Construction, vol. 2, Paris, pp. 83–94.

Bulychev, S.I., 1999. Relation between the reduced and unreduced hardness in nanomicroindentation tests. Tech. Phys. 44, 775–781.

Bulychev, S.I., Alekhin, V.P., Shorshorov, M.Kh., Ternovskii, A.P., Shnyrev, G.D., 1975. Determination of Young's modulus according to indentation diagram. Ind. Lab. 41, 1409–1412.

Cheng, Y.-T., Cheng, C.-M., 2004. Scaling, dimensional analysis and indentation measurements. Mater. Sci. Eng. R 44, 91–149.

Cheng, Y.-T., Cheng, C.-M., 2005. Relationships between initial unloading slope, contact depth, and mechanical properties for conical indentation in linear viscoelastic solids. J. Mater. Res. 20, 1046–1053.

Cheng, L., Xia, X., Yu, W., Scriven, L.E., Gerberich, W.W., 2000. Flat punch indentation of viscoelastic material. J. Pol. Sci.: Part B: Polym. Phys. 38, 10–22.

Cheng, L., Xia, X., Scriven, L.E., Gerberich, W.W., 2005. Spherical-tip indentation of viscoelastic material. Mech. Mater. 37, 213–226.

Chudoba, T., Richter, F., 2001. Investigation of creep behaviour under load during indentation experiments and its influence on hardness and modulus results. Surf. Coat. Technol. 148, 191–198.

Delafargue, A., Ulm, F.-J., 2004. Material Invariant Properties of Shales: Nanoindentation and Microporoelastic Analysis. MIT-CEE Report R04-02, Cambridge, MA.

Doerner, M.F., Nix, W.D., 1986. A method for interpreting the data from depth-sensing indentation instruments. J. Mater. Res. 1, 601–609.

Feng, G., Ngan, A.H.W., 2002. Effects of creep and thermal drift on modulus measurement using depth-sensing indentation. J. Mater. Res. 17, 660–668.

Fischer-Cripps, A.C., 2004. A simple phenomenological approach to nanoindentation creep. Mater. Sci. Eng. A 385, 74–82.

Galanov, B.A., 1982. An approximate method for the solution of some two-body contact problems with creep in the case of an unknown contact area. Sov. Appl. Mech. 18, 711–718.

Galin, L.A., 1961. Contact Problems in Theory of Elasticity. In: Sneddon, I.N. (Ed.). North Carolina State College (Translated by H. Moss).

Hay, J.C., Bolshakov, A., Pharr, G.M., 1999. A critical examination of the fundamental relations used in the analysis of nanoindentation data. J. Mater. Res. 14, 2296–2305.

Hertz, H., 1882. On the contact of elastic solids. Zeitschrift fur die reine und angewandte Mathematik (in German) 92, 156–171, Miscellaneous paper by H. Hertz. Jones and Schott (Eds.), Macmillan, London, 1896.

Hunter, S.C., 1960. The Hertz problem for a rigid spherical indenter and a viscoelastic half-space. J. Mech. Phys. Solids 8, 219–234.

Lee, E.H., 1955. Stress analysis in visco-elastic bodies. Quart. Appl. Math. 13, 183–190.

Lee, E.H., Radok, J.R.M., 1960. The contact problem for viscoelastic bodies. J. Appl. Mech. 27, 438–444.

Love, A.E.H., 1939. Boussinesq's problem for a rigid cone. Quart. J. Math. 10, 161–175.

Nixon, F.E., 1965. Handbook of Laplace Transformation. Prentice Hall.

Oliver, W.C., Pharr, G.M., 1992. An improved technique for determining hardness and elastic modulus using load and displacement sensing indentation experiments. J. Mater. Res. 7, 1564–1583.

Oliver, W.C., Pharr, G.M., 2004. Measurement of hardness and elastic modulus by instrumented indentation: Advances in understanding and refinements to methodology. J. Mater. Res. 19, 3–20.

Radok, J.R.M., 1957. Visco-elastic stress analysis. Quart. Appl. Math. 15, 198–202.

Sneddon, I.N., 1965. The relation between load and penetration in the axi-symmetric Boussinesq problem for a punch of arbitrary profile. Ind. J. Eng. Sci. 3, 47–57.

Tabor, D., 1951. Hardness of Metals. Clarendon press, Oxford.

Ting, T.C.T., 1966. The contact stresses between a rigid indenter and a viscoelastic half-space. J. Appl. Mech. 88, 845–854.